Computational Mechanics 33 (2003) 2–14 © Springer-Verlag 2003
DOI 10.1007/s00466-003-0477-5

A meshfree method: meshfree weak–strong (MWS) form method, for 2-D solids

G. R. Liu, Y. T. Gu

Abstract A novel meshfree weak–strong (MWS) form method is proposed based on a combined formulation of both the strong-form and the local weak-form. In the MWS method, the problem domain and its boundary is represented by a set of distributed points or nodes. The strong form or the collocation method is used for all nodes whose local quadrature domains do not intersect with natural (Neumann) boundaries. Therefore, no numerical integration is required for these nodes. The local weak-form, which needs the local numerical integration, is only used for nodes on or near the natural boundaries. The locally supported radial point interpolation method and the moving least squares approximation are used to construct the meshfree shape functions. The final system matrix will be sparse and banded for computational efficiency. Numerical examples of two-dimensional solids are presented to demonstrate the efficiency, stability, accuracy and convergence of the proposed meshfree method.

Keywords Computational mechanics, Strong-form, Weak-form; Meshfree method, Meshless method, Collocation method, Numerical analysis

1 Introduction

In recent years, meshfree or meshless methods have been developed and used to solve partial differential equations (PDE). More and more researchers are devoting themselves to the research of the meshfree methods, due to the fact that there are still many difficult issues to be solved. A detailed review of meshfree methods can be found in the recent monograph by Liu (2002). Meshfree methods can be largely categorized into two major categories (Liu, 2002): meshfree methods based on strong forms (or short for meshfree strong-form methods), such as the meshfree collocation method (Zhang et al. 2001; Zong, 2003), and meshfree methods based on the weak forms (or short for meshfree weak-form methods), such as the element-free Galerkin (EFG) method (Belytschko et al. 1994), the point interpolation method (PIM) (Liu and Gu 2001a), etc. There are also meshfree methods based on the integral representation method for functional approximations, such as the particle methods, many of which are introduced in the book of Liu and Liu (2003).

The meshfree strong-form method has a long history of development. Compared with meshfree weak-form method, the meshfree strong-form method has following attractive advantages:

1) It is simple to implement;
2) It is computationally efficient;
3) It is the truly meshless method without using any mesh for both field variable approximation and integration.

Because of the above advantages, meshfree strong-form methods have been successfully used in computational mechanics. For example, they have been widely used in the analysis for problems of fluid mechanics. However, shortcomings of meshfree strong-form methods are also very obvious. They are often unstable and less accurate, especially for problems governed by partial differential equations with Neumann (derivative) boundary conditions, such as solid mechanics problems with stress (natural) boundary conditions. In the direct meshfree strong-form methods, Neumann boundary conditions are satisfied using a series of separate equations, which are different with the governing equations in the problem domains. The error induced from the boundaries cannot be efficiently controlled in meshfree strong-form methods. Hence, meshfree strong-form methods are unsuccessful in applications of solid mechanics.

On the other hand, meshfree weak-form methods are also proposed and developed. They are included: the diffuse element method (DEM) (Nayroles et al. 1992), the EFG method (Belytschko et al. 1994), the PIM (Liu and Gu 2001a), and so on. The following advantages of meshfree weak-form methods are very attractive.

1) They exhibit very good stability and excellent accuracy. The reason is that the weak form can smear the error over the integral domain and control the error level.
2) The Neumann (natural) boundary conditions can be naturally satisfied by the weak form (hence, the stress boundary conditions are often called the natural boundary conditions in these methods).

Therefore, meshfree weak-form methods have been successfully applied in problems of solid mechanics. However, in particular, the above-mentioned meshfree weak-form methods are "meshless" only in terms of the interpolation

Received: 5 February 2002 / Accepted: 21 July 2003
Published online: 20 November 2003

G. R. Liu, Y. T. Gu (✉)
Department of Mechanical Engineering,
Centre for Advanced Computations in Engineering Science,
National University of Singapore,
10 Kent Ridge Crescent, Singapore 119260
E-mail: mpeliugr@nus.edu.sg

of the field variables, as compared to the usual FEM. Most of them have to use background cells to integrate a weak form over the global problem domain. The numerical integration makes them computationally expensive, and the background mesh for integration is responsible for not being "truly" meshless. In order to alleviate the global integration background mesh, a group of meshfree methods based on the local Petrov-Galerkin weak forms (or short as meshfree local weak-form methods) are proposed and developed, such as the meshless local Petrov-Galerkin (MLPG) method (Atluri and Zhu, 1998, 2002; Atluri et al. 1999; Gu and Liu 2001a,c), the method of finite spheres (De and Bathe 2000), the local Boundary Integral Equation (LBIE) method (Zhu et al. 1998), the local point interpolation method (LPIM) developed based on the idea of MLPG (Gu and Liu 2001b; Liu and Gu 2001b,c; Liu et al. 2002), and so on.

In these meshfree local weak-form methods, local weak forms integrated in a regular-shaped local domain are used. The local integral domain can be as simple as possible (such as circles, ellipses, rectangles, or triangles in 2-D; spheres, rectangular parallelepipeds, or ellipsoids in 3-D) and can be automatically constructed. These meshfree local weak-form methods have obtained satisfactory results in analyses of solid mechanics and fluid mechanics (Atluri and Zhu 1998, 2000; Atluri et al. 1999; Gu and Liu 2001a,b,c; Wu et al. 2002).

However, the local weak form used in meshfree local weak-form methods can only solve a part problem of the numerical integration in meshfree weak-form methods. The numerical integration is still a burden for nodes on or near the boundaries with a complex shape. The local integration may be also computationally expensive for many practical problems.

The meshfree strong-form methods and the meshfree local weak-form methods have their own advantages and their own shortcomings in the same time. A question will be naturally asked "can we couple the local weak-form with the strong-form together in a proper manner to fully take their advantages and avoid their disadvantages and how?" Liu and Gu (2002) wanted to find a answer for this question. This paper addresses this question in details.

Close examination of the meshfree strong-form method and the meshfree local weak-form method, reviews the following facts.

1) The implementation scheme of these two types of meshfree methods is very similar. They all construct and assemble discrete equations node-by-node.
2) If the delta function is used as the weight function in the meshfree local weak-form method, it becomes the meshfree strong-form method.
3) In the meshfree strong-form method, the instability and computational error is mainly induced by the natural boundary condition. On the contrary, the natural boundary condition can be easily and exactly enforced using the local weak form.
4) The number of nodes on the natural boundary is less than that of the internal nodes and nodes on the essential boundary. In the meshfree local weak-form method, the most computational cost of numerical integrations comes from the integration of internal nodes and nodes on the essential boundary.

The above properties provide us a possibility to combine the local weak form and the strong form together to fully take their advantages and avoid their disadvantages. In this paper, a novel meshfree method, the meshfree weak–strong (MWS) form method, is proposed based on a combined formulation of both the strong and the local weak forms. In the MWS method, the problem domain and its boundary is represented by a set of distributed points or nodes. The strong form or collocation method is used for all nodes whose local quadrature domains do not intersect with natural boundaries. Therefore, there are no numerical integrations at all for these nodes. The local weak form is only used for nodes on or near the natural boundaries. The natural boundary conditions can then be easily imposed to produce stable and accurate solutions. The locally supported radial point interpolation method (RPIM) and the moving least squares (MLS) approximation is used to construct the shape functions. Numerical examples of two-dimensional solids are presented to demonstrate the efficiency, stability and accuracy of the proposed MWS method.

2
Meshfree shape function construction

A number of ways to construct shape functions have been proposed. In this section, a briefing of RPIM and MLS is given. More details can be found in the book by Liu (2002) that introduces standard ways for creating different types of shape functions as well as their properties. It should mention here that RPIM and MLS denote two techniques to construct meshfree shape functions.

2.1
Radial basis point interpolation method (RPIM)

RPIM interpolation form is written as:

$$u^h(\mathbf{x}) = \sum_{i=1}^{n} R_i(r) a_i + \sum_{j=1}^{m} p_j(\mathbf{x}) b_j \tag{1}$$

with the constraint condition

$$\sum_{i=1}^{n} p_{ij}(\mathbf{x}) a_i = 0, \quad j = 1 \ldots m \tag{2}$$

where $R_i(r)$ is the radial basis functions (RBF), n is the number of nodes in the neighborhood of $\mathbf{x}$,$p_j(\mathbf{x})$ is monomials in the space coordinates $\mathbf{x}^{\mathrm{T}} = [x, y]$, m is the number of polynomial basis functions, coefficients a_i and b_j are interpolation constants. In the radial basis function $R_i(r)$, the variable is only the distance, r, between the interpolation point $\mathbf{x}$ and a node $\mathbf{x}_i$.

There are a number of radial basis functions. Characteristics of radial functions have been widely investigated (Powell 1992; Wendland 1998; Liu 2002). In this paper, the following Multi-quadrics (MQ) radial basis is used.

$$R_i(\mathbf{x}) = (r_i^2 + C^2)^q \tag{3}$$

There are two parameters (C and q) will influence the performance of RPIM using the MQ radial basis function. C is defined as

$$C = \alpha_0 d_i \tag{4}$$

where α_0 is a dimensionless coefficient chosen, and d_i is a parameter of the nodal distance. For the regularly distributed nodal case, d_i is the shortest distance between node i and neighbor nodes. Effects of α_0 and q have been studied in detail in Liu's book (2002). In static analysis of 2-D solids, it has been found that $\alpha_0 = 1.0$ and $q = 1.03$ lead to good results for most problems considered (Liu 2002). Hence, $\alpha_0 = 1.0$ and $q = 1.03$ will also be used in this paper.

The second term of Eq. (1) consists of polynomials. To ensure invertible interpolation matrix of RBF, the polynomial that is added into RBF cannot be arbitrary (Schaback and Wendland 2000; Cheng et al. 2003). A low degree polynomial is often needed to augment RBF to guarantee the non-singularity of the matrix. Because of the characters of the MQ RBF that is used in the following computing, the linear polynomial can ensure an invertible interpolation matrix of RBF. In addition, the linear polynomial added into the RBF can also ensure linear consistence and improve the interpolation accuracy (Liu 2002). Hence, the linear polynomial can be added into the MQ RBF.

Coefficients a_i and b_i in Eq. (1) can be determined by enforcing Eq. (1) to be satisfied at the n nodes surrounding point $\mathbf{x}$. Equation (1) can be re-written in matrix form as follows

$$\begin{bmatrix} \mathbf{u} \\ \mathbf{0} \end{bmatrix} = \begin{bmatrix} \mathbf{R}_0 & \mathbf{P}_m \\ \mathbf{P}_m^{\mathrm{T}} & \mathbf{0} \end{bmatrix} \begin{bmatrix} \mathbf{a} \\ \mathbf{b} \end{bmatrix} = \mathbf{G}\mathbf{a}_0 \tag{5}$$

where

$$\mathbf{P}_m^{\mathrm{T}} = \begin{bmatrix} 1 & 1 & \cdots & 1 \\ x_1 & x_2 & \cdots & x_n \\ y_1 & y_2 & \cdots & y_n \end{bmatrix},$$

$$\mathbf{R}_0 = \begin{bmatrix} B_1(r_1) & B_2(r_1) & \cdots & B_n(r_1) \\ B_1(r_2) & B_2(r_2) & \cdots & B_n(r_2) \\ \cdots & \cdots & \cdots & \cdots \\ B_1(r_n) & B_2(r_n) & \cdots & B_n(r_n) \end{bmatrix} \tag{6}$$

$$\mathbf{a}_0^{\mathrm{T}} = [a_1, a_2, \cdots, a_n, b_1, b_2, b_3,] \tag{7}$$

Because the matrix $\mathbf{R}_0$ is symmetric, the matrix $\mathbf{G}$ will also be symmetric. In order to avoid computing inversion matrix $\mathbf{G}^{-1}$, the following algorithm to solve Eq. (5) can be used. From Eq. (1), we have

$$\mathbf{a} = \mathbf{R}_0^{-1}\mathbf{u}_e - \mathbf{R}_0^{-1}\mathbf{P}_m\mathbf{b} \tag{8}$$

Substituting of the above expression into Eq. (2) gives

$$\mathbf{b} = \mathbf{S}_b\mathbf{u}_e \tag{9}$$

where

$$\mathbf{S}_b = [\mathbf{P}_m^{\mathrm{T}}\mathbf{R}_0^{-1}\mathbf{P}_m]^{-1}\mathbf{P}_m^{\mathrm{T}}\mathbf{R}_0^{-1} \tag{10}$$

Substituting Eq. (9) back into Eq. (8), we obtain

$$\mathbf{a} = \mathbf{S}_a\mathbf{u}_e \tag{11}$$

where

$$\mathbf{S}_a = \mathbf{R}_0^{-1}[1 - \mathbf{P}_m\mathbf{S}_b] \tag{12}$$

The interpolant Eq. (1) is finally expressed as

$$u(\mathbf{x}) = [\mathbf{R}^{\mathrm{T}}(\mathbf{x})\mathbf{S}_a + \mathbf{p}^{\mathrm{T}}(\mathbf{x})\mathbf{S}_b]\mathbf{u}_e = \mathbf{\Phi}(\mathbf{x})\mathbf{u}_e \tag{13}$$

where the shape function $\mathbf{\Phi}(\mathbf{x})$ is defined by

$$\mathbf{\Phi}(\mathbf{x}) = [\phi_1(\mathbf{x}), \phi_2(\mathbf{x}), \cdots, \phi_n(\mathbf{x})] = \mathbf{R}^{\mathrm{T}}(\mathbf{x})\mathbf{S}_a + \mathbf{p}^{\mathrm{T}}(\mathbf{x})\mathbf{S}_b \tag{14}$$

Mathematicians have proven the existence of the radial interpolation for arbitrary scattered nodes (Schaback and Wendland 2000). Therefore, RPIM usually has no interpolation singularity problem.

It can be found from above discussion that RPIM passes through the nodal values. Therefore, RPIM shape functions given in Eq. (14) satisfy the Kronecker delta condition. Thus,

$$\phi_i(\mathbf{x}_j) = \delta_{ij} = \begin{cases} 1 & i = j \\ 0 & i \neq j \end{cases} \tag{15}$$

2.2 Moving least squares (MLS) approximation

The MLS interpolant (Lancaster and Salkauskas 1986) $u^h(x)$ is defined in the domain Ω by

$$u^h(\mathbf{x}) = \sum_{j=1}^{m} p_j(\mathbf{x})a_j(\mathbf{x}) = \mathbf{p}^{\mathrm{T}}(\mathbf{x})\mathbf{a}(\mathbf{x}) \tag{16}$$

where m is the number of basis functions, the coefficient $a_j(x)$ in Eq. (16) is also functions of $\mathbf{x}$; $\mathbf{p}(\mathbf{x})$ is the polynomial basis; $\mathbf{a}(\mathbf{x})$ is obtained at any point $\mathbf{x}$ by minimizing a weighted discrete $\mathbf{L}_2$ norm of:

$$J = \sum_{i=1}^{n} w(\mathbf{x} - \mathbf{x}_i)[\mathbf{p}^{\mathrm{T}}(\mathbf{x}_i)\mathbf{a}(\mathbf{x}) - u_i]^2 \tag{17}$$

where n is the number of nodes in the neighborhood of $\mathbf{x}$ for which the weight function $w(\mathbf{x} - \mathbf{x}_i) \neq 0$, and u_i is the nodal value parameter of u at $\mathbf{x} = \mathbf{x}_i$.

Using the stationarity condition for J with respect to $\mathbf{a}(\mathbf{x})$, we can solve $\mathbf{a}(\mathbf{x})$. And then, substituting it into Eq. (16), we have

$$u^h(\mathbf{x}) = \sum_{i=1}^{n} \phi_i(\mathbf{x})u_i \tag{18}$$

where the MLS shape function $\phi_i(\mathbf{x})$ is defined by

$$\phi_i(\mathbf{x}) = \sum_{j=1}^{m} p_j(\mathbf{x})(\mathbf{A}^{-1}(\mathbf{x})\mathbf{B}(\mathbf{x}))_{ji} \tag{19}$$

where $\mathbf{A}(\mathbf{x})$ and $\mathbf{B}(\mathbf{x})$ are the matrices defined by

$$\mathbf{A}(\mathbf{x}) = \sum_{i=1}^{n} w_i(\mathbf{x})\mathbf{p}^{\mathrm{T}}(\mathbf{x}_i)\mathbf{p}(\mathbf{x}_i), \quad w_i(\mathbf{x}) = w(\mathbf{x} - \mathbf{x}_i) \tag{20}$$

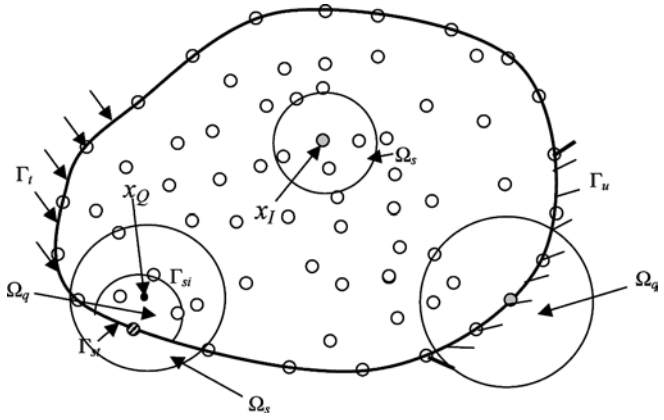

Fig. 1. To analyze a problem using MWS: the local support domain Ω_s, local quadrature domain Ω_q

$$\mathbf{B}(\mathbf{x}) = [w_1(\mathbf{x})\mathbf{p}(\mathbf{x}_1), w_2(\mathbf{x})\mathbf{p}(\mathbf{x}_2), \ldots, w_n(\mathbf{x})\mathbf{p}(\mathbf{x}_n)] \tag{21}$$

It can be found from above discussion that the MLS approximation does not pass through the nodal values. Therefore the MLS shape functions given in Eq. (19) do not, in general, satisfy the Kronecker delta condition.

3
Strong–weak form for 2-D solids

Consider the following two-dimensional problem of solid mechanics in a domain Ω bounded by Γ, as shown in Fig. 1:

$$\sigma_{ij,j} + b_i = 0 \quad \text{in } \Omega \tag{22}$$

where σ_{ij} is the stress tensor, which corresponds to the displacement field u_i, b_i is the body force tensor, and $()_{,i}$ denotes $\partial/\partial x_i$. The boundary conditions are given as follows:

$$\sigma_{ij}n_j = \bar{t}_i \quad \text{on the natural boundary } \Gamma_t \tag{23}$$

$$u_i = \bar{u}_i \quad \text{on the essential boundary } \Gamma_u \tag{24}$$

in which the $\bar{u}_i$ and $\bar{t}_i$ denote the prescribed displacements and tractions, respectively, and n_j is the unit outward normal to domain Ω.

3.1
Strong form for internal nodes and nodes on essential boundaries

As shown in Fig. 1, the problem domain and boundaries are represented by properly scattered nodes. The key idea of the MWS method is that in establishing the discrete system equations, both the strong form and the local weak form are used for the same problem, but for different nodes. In Fig. 1, Ω_q is the local quadrature domain for a field node. If Ω_q does not intersect with the natural boundaries, the strong form is used for this node. Otherwise, the local weak form is used.

For an internal node or a node on the essential boundary, whose local quadrature domain does not intersect with the natural boundary, the following strong form is used.

$$\begin{aligned} \frac{E}{1-\nu^2}\left(\frac{\partial^2 u}{\partial x^2} + \frac{1-\nu}{2}\frac{\partial^2 u}{\partial y^2} + \frac{\partial^2 v}{\partial x \partial y}\right) + b_x = 0 \\ \frac{E}{1-\nu^2}\left(\frac{\partial^2 v}{\partial y^2} + \frac{1-\nu}{2}\frac{\partial^2 v}{\partial x^2} + \frac{\partial^2 u}{\partial x \partial y}\right) + b_y = 0 \end{aligned} \tag{25}$$

where E and ν are Young's modulus and Poisson ratio, b_x and b_y are body forces at x direction and y direction, respectively.

3.2
Local weak form for nodes on natural boundaries

A generalized local weak form of the partial differential Equation (22), over a local quadrature domain Ω_q bounded by Γ_q, can be obtained using the weighted residual method

$$\int_{\Omega_q} w_i(\sigma_{ij,j} + b_i)\mathrm{d}\Omega - \int_{\Gamma_{qu}} \alpha w_i(u_i - \bar{u}_i)\mathrm{d}\Gamma = 0 \tag{26}$$

where w_i is the weight function. It should note here that the last term in (26) is to enforce the essential boundary condition. If RPIM shape functions are used, this term does not need. However, if MLS shape functions are used, this term is necessary.

The first term on the left hand side of Eq. (26) can be integrated by parts to become

$$\int_{\Gamma_q} w_i\sigma_{ij}n_j\,\mathrm{d}\Gamma - \int_{\Omega_q}(w_{i,j}\sigma_{ij} - w_i b_i)\mathrm{d}\Omega - \int_{\Gamma_{qu}} \alpha w_i(u_i - \bar{u}_i)\mathrm{d}\Gamma = 0 \tag{27}$$

The local quadrature domain Ω_q of a node x_i is a domain in which $w_i(x) \neq 0$. An arbitrary shaped local quadrature domain can be used. A circle or rectangular quadrature domain is used in this paper for convenience. It can be found that the boundary Γ_s for the local quadrature domain usually comprises three parts: the internal boundary Γ_{qi}, the boundaries Γ_{qu} and Γ_{qt}, over which the essential and natural boundary conditions are specified. Imposing the natural boundary condition and noticing that $\sigma_{ij}n_j = \partial u/\partial n \equiv t_i$ into Eq. (27), it is obtained that

$$\int_{\Gamma_{si}} w_i t_i\,\mathrm{d}\Gamma + \int_{\Gamma_{su}} w_i t_i\,\mathrm{d}\Gamma + \int_{\Gamma_{st}} w_i\bar{t}_i\,\mathrm{d}\Gamma - \int_{\Omega_s}(w_{i,j}\sigma_{ij} - w_i b_i)\mathrm{d}\Omega - \int_{\Gamma_{qu}} \alpha w_i(u_i - \bar{u}_i)\mathrm{d}\Gamma = 0 \tag{28}$$

And then, we can obtain

$$\int_{\Omega_q} w_{i,j}\sigma_{ij}\,\mathrm{d}\Omega + \int_{\Gamma_{qu}} \alpha w_i u_i\,\mathrm{d}\Gamma - \int_{\Gamma_{si}} w_i t_i\,\mathrm{d}\Gamma - \int_{\Gamma_{su}} w_i t_i\,\mathrm{d}\Gamma = \int_{\Gamma_{st}} w_i\bar{t}_i\,\mathrm{d}\Gamma + \int_{\Omega_s} w_i b_i\,\mathrm{d}\Omega + \int_{\Gamma_{qu}} \alpha w_i\bar{u}_i\,\mathrm{d}\Omega \tag{29}$$

Using Eq. (28) for any node $\mathbf{x}_i$, instead of dealing with a global boundary value problem, the problem becomes a localized boundary value problem over a local quadrature domain. In the present formulation, the equilibrium equation and boundary conditions are satisfied in all local quadrature domains Ω_q and on their boundary Γ_q. Although the quadrature domains affect the solution, as long as the union of all the local quadrature domains covers the global domain Ω, the equilibrium equation and the boundary conditions will theoretically be satisfied in the global domain Ω and in its boundary Γ (Atluri and Zhu 1998; Liu and Gu 2001b).

The test (weight) function plays an important role in the performance of the local weak form. Theoretically, any weight function is acceptable as long as the condition of continuity is satisfied. However, it has been found that test functions which decrease in magnitude with increasing distance from the sampling point $\mathbf{x}_Q$ to the node $\mathbf{x}_i$ yield better results. Therefore, test functions, which only depend on the distance between the two points, are considered. Following the idea of the Galerkin FEM, the test functions can also be constructed by RPIM or MLS (Liu 2002). In order to simplify, we can deliberately select the test functions such that they vanish over Γ_{qi}, although it is not necessary. This can be easily satisfied using the following 4th-order spline weight function.

$$w_i(x) = \begin{cases} 1 - 6\left(\frac{d_i}{r_w}\right)^2 + 8\left(\frac{d_i}{r_w}\right)^3 - 3\left(\frac{d_i}{r_w}\right)^4 & 0 \le d_i \le r_w \\ 0 & d_i \ge r_w \end{cases} \tag{30}$$

where $d_i = |x_Q - x_i|$ is the distance from node x_i to point x_Q, and r_w is the size of the support for the weight function. Hence, Eq. (29) can be simplified because the integration along the internal boundary Γ_{qi} vanishes. Equation (29) can be re-written as:

$$\int_{\Omega_q} w_{i,j}\sigma_{ij}\,\mathrm{d}\Omega + \int_{\Gamma_{qu}} \alpha w_i u_i\,\mathrm{d}\Gamma - \int_{\Gamma_{qu}} w_i t_i\,\mathrm{d}\Gamma = \int_{\Gamma_{qt}} w_i \bar{t}_i\,\mathrm{d}\Gamma + \int_{\Omega_q} w_i b_i\,\mathrm{d}\Omega + \int_{\Gamma_{qu}} \alpha w_i \bar{u}_i\,\mathrm{d}\Omega \tag{31}$$

3.3 Discrete formulations and the numerical implementations

The global problem domain Ω is represented by distributed nodes. Using RPIM equation (13) or MLS equaton (18), respectively, we can get

$$\mathbf{u}(\mathbf{x}) = \begin{Bmatrix} \mathbf{u} \\ v \end{Bmatrix} = \sum_{j=1}^{n} \begin{bmatrix} \phi_j & 0 \\ 0 & \phi_j \end{bmatrix} \begin{Bmatrix} u_j \\ v_j \end{Bmatrix} = \sum_{j=1}^{n} \mathbf{\Phi}_j \mathbf{u}_j \tag{32}$$

where $\mathbf{u}_e$ is the vector of nodal displacements, $\boldsymbol{\psi}$ is the matrix of shape functions. Substituting Eq. (32) into the strong form, Eq. (25) and local weak form (29) for all nodes leads to the following discrete equations

$$\mathbf{KU} = \mathbf{F} \tag{33}$$

where $\mathbf{U}$ is the vector of displacements for all nodes in the entire problem domain. $\mathbf{K}$ and $\mathbf{F}$ are defined as

$$\mathbf{K}_{ij} = \begin{cases} \int_{\Omega_q} \widehat{\mathbf{v}}_i^{\mathrm{T}}(\mathbf{x}, \mathbf{x}_i)\mathbf{D}\mathbf{B}_j(\mathbf{x})\mathrm{d}\Omega - \int_{\Gamma_{qi}} \widehat{\mathbf{w}}(\mathbf{x}, \mathbf{x}_i)\mathbf{N}\mathbf{D}\mathbf{B}_j(\mathbf{x})\mathrm{d}\Gamma \\ \quad - \int_{\Gamma_{qu}} \widehat{\mathbf{w}}(\mathbf{x}, \mathbf{x}_i)\mathbf{N}\mathbf{D}\mathbf{B}_j(\mathbf{x})\mathrm{d}\Gamma \\ \quad + \alpha \int_{\Gamma_{qu}} \widehat{\mathbf{w}}(\mathbf{x}, \mathbf{x}_\mathbf{i})\mathbf{\Phi}_j(\mathbf{x})\mathrm{d}\Gamma, & \Omega_q(\mathbf{x}_i) \cap \Gamma_t \neq \emptyset \\ \mathbf{L}^{\mathrm{T}}\mathbf{D}\mathbf{L}\,\mathbf{\Phi}_j(\mathbf{x}_i), & \Omega_q(\mathbf{x}_i) \cap \Gamma_t = \emptyset \end{cases} \tag{34}$$

$$\mathbf{F}_i(t) = \int_{\Gamma_{qt}} \widehat{\mathbf{w}}(\mathbf{x}, \mathbf{x}_i)\bar{\mathbf{t}}\,\mathrm{d}\Gamma + \int_{\Gamma_q} \widehat{\mathbf{w}}(\mathbf{x}, \mathbf{x}_i)\mathbf{b}\,\mathrm{d}\Omega + \alpha \int_{\Gamma_{qu}} \widehat{\mathbf{w}}(\mathbf{x}, \mathbf{x}_i)\bar{\mathbf{u}}\,\mathrm{d}\Gamma, \quad \Omega_q(\mathbf{x}\bar{\mathbf{u}}) \cap \Gamma_t \neq \emptyset \tag{35}$$

with $\widehat{\mathbf{w}}(\mathbf{x}, \mathbf{x}_i)$ being the value of the weight function matrix, corresponding to node i, evaluated at the point $\mathbf{x}$, $\mathbf{\Phi}_j$ is the matrix of shape functions, and

$$\mathbf{N} = \begin{bmatrix} n_x & 0 & n_y \\ 0 & n_y & n_x \end{bmatrix}, \tag{36}$$

$$\mathbf{B}_j(\mathbf{x}) = \begin{bmatrix} \phi_{j,x}(\mathbf{x}) & 0 \\ 0 & \phi_{j,y}(\mathbf{x}) \\ \phi_{j,y}(\mathbf{x}) & \phi_{j,x}(\mathbf{x}) \end{bmatrix}, \tag{37}$$

$$\widehat{\mathbf{w}}(\mathbf{x}, \mathbf{x}_i) = \begin{bmatrix} \widehat{\mathbf{w}}(\mathbf{x}, \mathbf{x}_i) & 0 \\ 0 & \widehat{\mathbf{w}}(\mathbf{x}, \mathbf{x}_i) \end{bmatrix}, \tag{38}$$

$$\widehat{\mathbf{v}}_i(\mathbf{x}, \mathbf{x}_i) = \begin{bmatrix} \widehat{\mathbf{w}}_{i,x}(\mathbf{x}, \mathbf{x}_i) & 0 \\ 0 & \widehat{\mathbf{w}}_{i,y}(\mathbf{x}, \mathbf{x}_i) \\ \widehat{\mathbf{w}}_{i,y}(\mathbf{x}, \mathbf{x}_i) & \widehat{\mathbf{w}}_{i,x}(\mathbf{x}, \mathbf{x}_i) \end{bmatrix} \tag{39}$$

where (n_x, n_y) is the unit outward normal to the boundary Γ_q, $\mathbf{L}$ is the differential operator matrix, $\mathbf{D}$ is the stress–strain matrix as given in follows.

$$\mathbf{L} = \begin{bmatrix} \frac{\partial}{\partial x} & 0 \\ 0 & \frac{\partial}{\partial y} \\ \frac{\partial}{\partial y} & \frac{\partial}{\partial x} \end{bmatrix}, \tag{40}$$

$$\mathbf{D} = \frac{E}{1-\nu^2} \begin{bmatrix} 1 & \nu & 0 \\ \nu & 1 & 0 \\ 0 & 0 & (1-\nu)/2 \end{bmatrix}, \quad \text{for plane stress} \tag{41}$$

From Eq. (34), it can be easily seen that the system "stiffness matrix" $\mathbf{K}$ in the present methods is banded because the support domain is compact. However, $\mathbf{K}$ is usually asymmetric. The asymmetry is caused by the use of the weak–strong forms. In addition, the asymmetric boundary integration of $\mathbf{K}$ in Eq. (34) also leads to asymmetry of $\mathbf{K}$.

For nodes are located on the natural boundaries, the local weak forms are used. Therefore, as shown in Fig. 1, for a node $\mathbf{x}_i$, there exist two local domains:

a) the local quadrature domain Ω_q for node $\mathbf{x}_i$ (size r_q) for numerical integration;
b) the support domain Ω_s for $\mathbf{x}_Q$ (size r_s) for construction shape functions.

These two local domains are independent. The size of the local quadrature domain (r_q) for node i and the size of the support domain (r_s) are defined as

$$r_q = \alpha_q d_i \tag{42}$$

$$r_s = \alpha_s d_i \tag{43}$$

where, α_q and α_s are coefficients chosen. d_i is a parameter of the distance between the node i and neighbor nodes.

For internal nodes that use the strong forms, as shown in Fig. 1, there is only one local domain: the support domain Ω_s, needed. The size of the local support domain has been defined in Eq. (43).

Although a part of nodes need numerical integrations and integrations in the present method are only performed in regular-shaped local quadrature domains, attentions are still needed to obtain the exact numerical integration. The Ω_q is divided into small regular partitions and sufficient Gauss quadrature points should be used in each small partition. A detailed discussion of local numerical integrations can be seen in the book of Liu (2002).

3.4
The flowchart

The flowchart of the MWS method can be given briefly as follows:

1 loop over all nodes of the problem domain
  2 construct the local quadrature domain for the node i
  3 if the local quadrature domain intersects with the natural boundaries, then
    3.1 loop over quadrature points x_Q in the local quadrature domain
      a. compute shape function based on the local support domain;
      b. evaluate contributions to equation using the local weak form;
    3.2 end loop of local quadrature domain
    3.3 go to 1
  4 else, if the local quadrature does not intersect with the natural boundaries, then
    4.1 compute shape function based on the local support domain;
    4.2 evaluate contributions to equation using the strong form;
    4.3 go to 1
5 end loop for nodes
6 solve system equation to get results.

4
Numerical examples

Several numerical examples of two-dimensional elastostatics are studied to examine the efficiency and performance of the MWS method.

It should be noted here that there is a locking problem in the incompressible case when $\nu \approx 0.5$. As one of advantages for mesh-free method (e.g. EFG), it has been claimed that the mesh-free methods are locking-free in incompressible analysis. However, these conclusions were drawn primarily by only studying the analysis results of a few example problems and not considering the inf-sup condition. Recently, it has been reported that the mesh-free method (e.g. EFG) does indeed suffer from locking in incompressible deformations. De and Bathe (De and Bathe 2001) found this problem and studied it in very detail (Bathe 2001; De and Bathe 2001). However, in our studies, $\nu = 0.25$ or $\nu = 0.3$ is used in the following numerical examples. Hence, incompressible conditions are not considered.

4.1
Standard patch test

The first numerical example is the standard patch test. Three patches shown in Fig. 2 are tested. Figure 2a shows a patch with 15 irregular distributed nodes. Figure 2b shows a patch of 25 nodes including nine irregularly-placed interior nodes. Figure 2c shows a patch of 55 nodes including 39 irregularly distributed internal nodes.

The dimensions of these patch tests are listed in figures. The parameters are taken as $E = 1.0$ and $\nu = 0.3$. In these patch tests, the displacements are prescribed on all outside boundaries by a linear function of x and y:

$$u_i = x_i + y_i, \quad v_i = x_i - y_i \ , \tag{44}$$

Satisfaction of the patch test requires that the displacement of any interior node be given by the same linear functions and that the strains and stresses be constant in the patch. Because there is no natural boundary in the patch test, all nodes use strong forms to construct the system equation. $\alpha_s = 1.6$ (defined in Eq. (43)) is used for the support domain. Both RPIM (added linear polynomial terms) and MLS shape function are used.

The MWS method can exactly pass all patch tests. If RPIM shape functions are used, the relative displacements error less than 10^{-15}. If MLS shape functions are used, the relative displacements error, which is mainly affected by the penalty coefficient chosen for the enforcement of essential boundary conditions, less than 10^{-6}.

It should be mentioned here the requirements for the numerical method based on the weak -strong forms to pass the patch test are listed as follows (Liu 2002):

1) The shape functions are of at least linear consistency;
2) The essential boundary conditions have to be accurately imposed;
3) Accurate numerical operations are required, such as the numerical integration.

The last requirement can be easily satisfied in the present method. All nodes use strong forms to construct system equation. No numerical integrations are used at all. The accurate numerical operations can be easily ensured.

RPIM (added the linear polynomial term) and MLS shape functions can satisfy the first requirement easily because linear polynomials are included in the basis. Without linear terms, RPIM shape functions do not satisfy the first requirement. Hence, it will leads to error in these patch tests.

RPIM shape function can also satisfy the third requirement, as it possesses the Kronecker delta function property. However, the MLS shape function has no delta

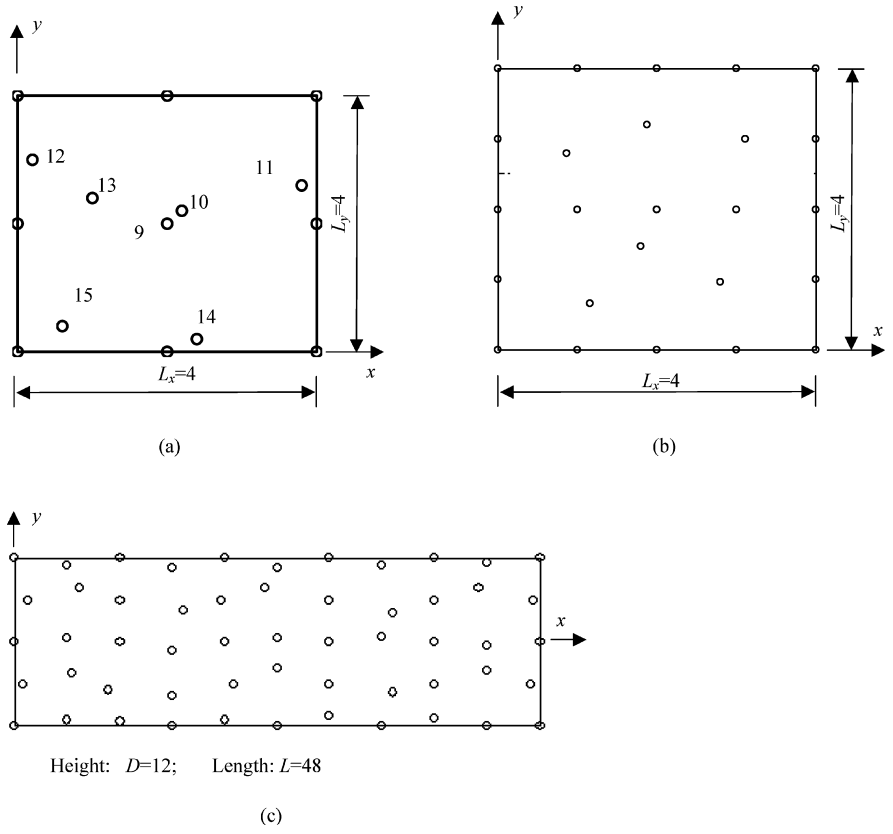

Fig. 2. Patch tests **a** a patch with 15 irregular nodes **b** a patch with 25 irregular nodes **c** a patch with 55 irregular nodes

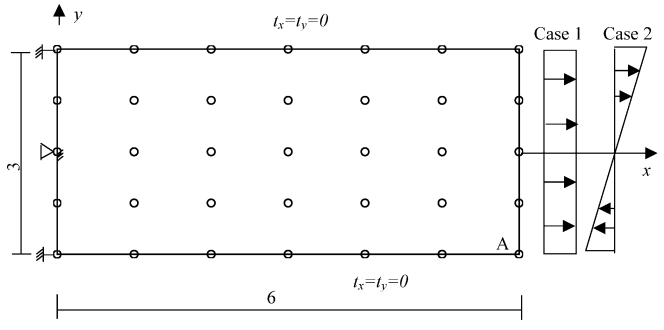

Fig. 3. A higher-order patch and regular nodal distribution

function properties. The second requirement cannot be exactly satisfied when MLS shape function is used. The penalty method is used in this paper to enforce the essential boundary conditions. Although MWS can pass the standard patch test, the penalty method will induce to numerical error. Hence, for the standard patch test problem, the error of MWS using MLS is larger than that of MWS using RPIM.

4.2 Higher-order patch test

In the above examples, there is no natural boundary condition. Hence, no local weak-form is used. In order to test the efficiency of the combination of weak–strong forms, the following high-order patch tests are studied.

As shown in Fig. 3, a patch is subjected to two types of loading at the right end.

1) Case 1: a uniform axial stress of unit intensity is applied on the right end. The exact solution for this problem with $E = 1$ and $\nu = 0.25$ is:

$$u_i = x_i, \quad v_i = y_i/4 \ , \tag{45}$$

2) Case 2: a linearly varying normal stress is applied on the right end. The exact solution for this problem with $E = 1$ and $\nu = 0.25$ is:

$$u_i = xy/3, \quad v_i = -(x^2 + y^2/4)/3 \ , \tag{46}$$

For construction of shape functions, the support domains in RPIM and MLS with $\alpha_s = 2.5$ are used. It can be found that case 1 is passed exactly by the presented MWS method using both RPIM (added the linear polynomial terms) and MLS. In the case 1, it demonstrates that the MWS method exactly implement the natural (force) boundary condition and lead to an exact solution for this problem whose analytical displacement solution is a linear function.

The computational results for case 2 are shown in Table 1. In the analysis of case 2, the second order ($m = 6$) basis is used in MLS and the linear polynomial is added in RPIM. It can be seen that there exist error in solving the case 2 by the MWS method using both RPIM and MLS shape functions.

The reason for the computational error mainly comes from the errors of numerical implementations: the numerical integrations. In order to study the effect of numerical integration, two different sizes of quadrature domains are used and listed in Table 1. It can be found that the error will decrease when a lager quadrature

Table 1. Relative errors (%) of u_x at point A for higher-order patch test case 2 (using regular nodes)

	$\alpha_q = 1.0$		$\alpha_q = 1.5$	
	u	v	u	v
MWS (RPIM)	−6.68 (11.36%)	−13.79 (13.17%)	−6.09 (1.64%)	−12.57 (3.15%)
LRPIM	−6.40 (6.71%)	−13.10 (7.48%)	−6.07 (1.21%)	−12.54 (2.92%)
MSW (MLS)	−5.95 (−0.75%)	−12.11 (−0.61%)	−5.97 (−0.45%)	−12.14 (−0.38%)
MLPG	−5.95 (−0.72%)	−12.12 (−0.57%)	−5.98 (−0.24%)	−12.16 (−0.19%)
Exact	−6.00	−12.18	−6.00	−12.18

domain is used. When $\alpha_q = 1.0$, the local quadrature domain is too small to smears the error along the natural boundary. It can also be found that the accuracy of the solution improves with the improvement of the numerical integration by use of more Gauss quadrature points and sub-divisions for integration.

The irregularly distributed nodes, as shown in Fig. 4, are also used. Results are listed in Table 2. It can be found that the MWS method can obtain good results for this irregularly nodal distribution.

For comparison, results by local radial point interpolation method (LRPIM) and MLPG methods, which are meshfree local weak-form methods using local weak forms for all field nodes, are also obtained and listed in Tables 1 and 2. It can be seen that LRPIM and MLPG methods usually lead to more accurate results than the MWS method because of the higher accuracy of the weak form method.

The purely meshfree collocation method that uses strong forms for all nodes is also used to get results for the high order patch test. It has been found that the collocation method can also get satisfactory results for the case 1, whose force boundary condition is simple. However, it leads to big errors ($> 15\%$) for the case 2. Displacement results of irregular nodes using meshfree collocation method and RPIM is also listed in Table 2. The error is more than 40%. The solution of the collocation method is also instable. It is sensitive to the nodal distribution and computational parameters. The error and instability mainly come from the error of the implementation of the complex force boundary condition in the case 2. Compared with the purely collocation method, the present MWS method has good accuracy and stability for this high order patch test.

Results of several meshfree methods above used for patch tests are summarized in Table 3.

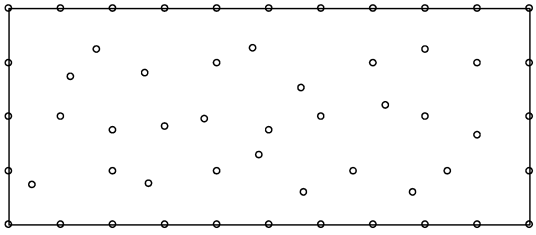

Fig. 4. The irregular nodal distribution for the high order patch test

4.3 Cantilever beam

The cantilever beam shown in Fig. 5 is considered. The beam is of length L and height D subjected to a parabolic traction at the free end. The beam has a unit thickness and a plane stress problem is considered. This is a benchmark problem because the analytical solution is available. The analytical displacements are given by

$$u_x = -\frac{Py}{6EI}\left[(6L - 3x)x + (2 + v)\left(y^2 - \frac{D^2}{4}\right)\right] \quad (47)$$

$$u_y = -\frac{P}{6EI}\left[3vy^2(L - x) + (4 + 5v)\frac{D^2 x}{4} + (3L - x)x^2\right] \quad (48)$$

Table 2. Relative errors (%) of u_x at point A for higher-order patch test case 2 (using irregular nodes)

	Exact	MWS (RPIM)	LRPIM	Collocation (RPIM)	MWS (MLS)	MLPG
u	−6.00	−6.38	−5.95	−8.78	−5.97	−5.98
Error	/	6.49%	−0.81%	46.60%	−0.39%	−0.29%
v	−12.18	−13.23	−12.02	−16.20	−12.16	−12.17
Error	/	8.58%	−1.41%	49.30%	−0.16%	−0.16%

Table 3. Summarization of patch tests

	Standard patch test	Higher-order patch test (case 1)	Higher-order patch test (case 2)
MWS(RPIM)	Pass	Pass	Pass with small error
MWS(MLS)	Pass	Pass	Pass with small error
LRPIM	Pass	Pass	Pass with small error
MLPG	Pass	Pass	Pass with small error
Collocation method	Pass	Pass	Cannot pass

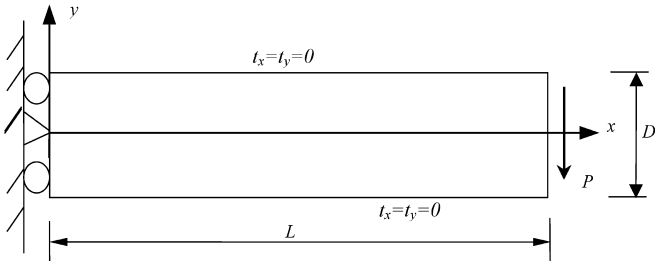

Fig. 5. A cantilever beam and boundary conditions

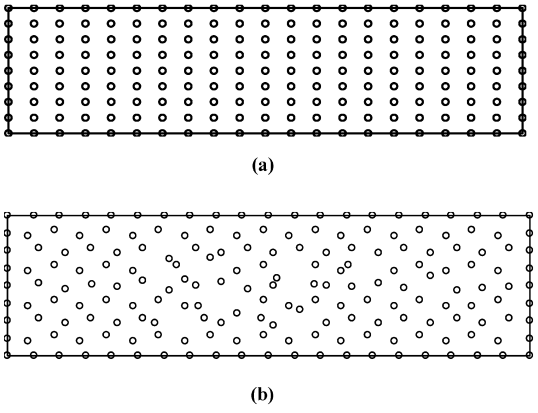

Fig. 6 a Regular distribution of nodes for cantilever beam. **b** Irregular distribution of nodes for cantilever beam

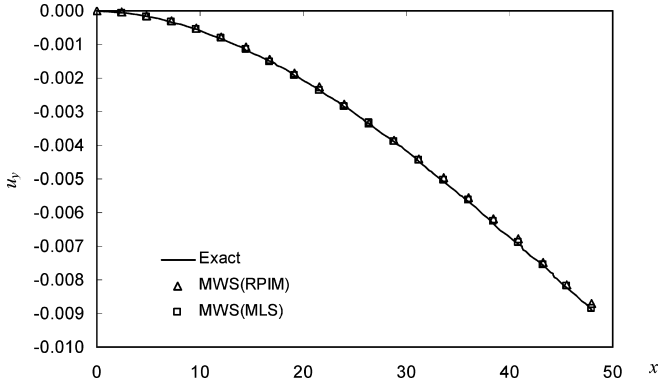

Fig. 7. Displacement (u_y) of the beam along $y = 0$ using 189 regular nodes

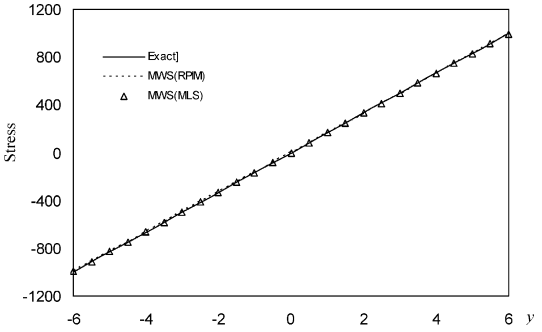

Fig. 8. Stress (σ_{xx}) of the beam along $x = L/2$ using 189 regular nodes

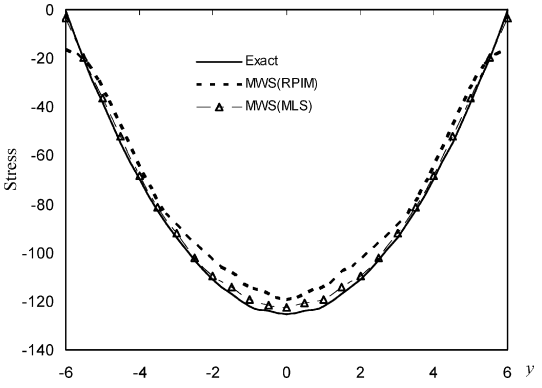

Fig. 9. Stress (τ_{xx}) of the beam along $x = L/2$ using 189 regular nodes

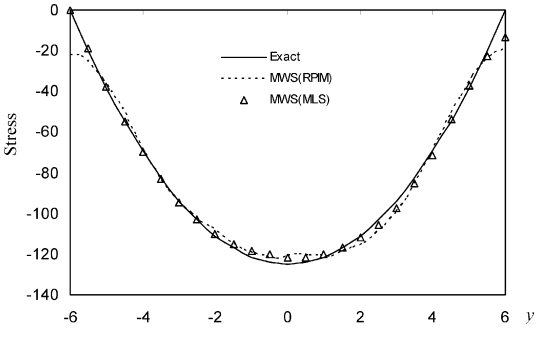

Fig. 10. Stress (τ_{xx}) of the beam along $x = L/2$ using 189 irregular nodes

The stress components can also be obtained. The parameters are taken as $E = 3.0 \times 10^7, v = 0.3, D = 12, L = 48,$ and $P = 1000$. Both regular and irregular distributions of nodes as shown in Fig. 6 are employed. In the analyses of this beam, the second order $(m = 6)$ basis is used in MLS and the linear polynomial is added in RPIM.

(a) Numerical results

Figure 7 shows a comparison of the analytical solution and the MWS solution for the beam deflection along the x -axis. The plot shows excellent agreement between the analytical and numerical results. Figures 8 and 9 illustrates the comparison between the stresses σ_x and τ_{xy} at the section $x = L/2$ calculated analytically and using the MWS methods using regular 189 nodes. Very good agreement is observed. The irregularly distributed nodes are also used to obtain the solutions. Figure 10 illustrates the comparison between the shear stress τ_{xy} at the section $x = L/2$ calculated analytically and using the MWS methods. Again, very good agreement is observed for these irregular distributions of nodes.

The meshfree collocation method that uses purely strong forms is also used to get results for this problem. It has been found that the collocation method leads to big errors for this problem. It even fails for the irregular nodal distribution. The solution of the collocation method is also instable. Compared with the purely collocation method, the present MWS method has good accuracy and stability for this problem.

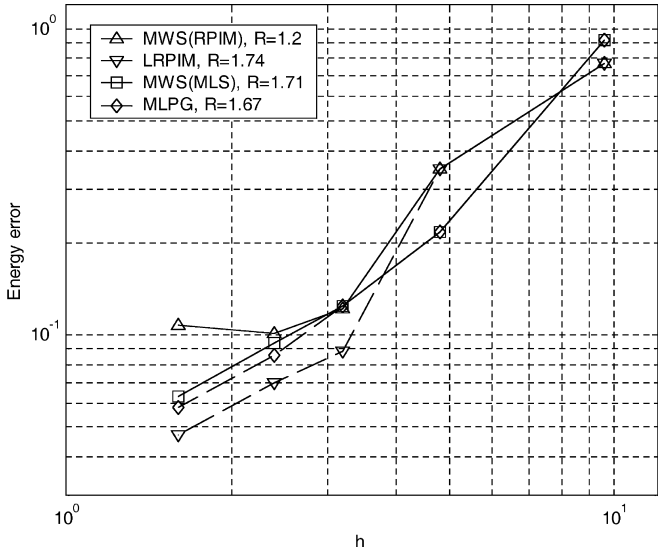

Fig. 11. Convergence in energy norm

For the error analysis, the following energy norm is defined as the error indicator, as the accuracy in strain or stress is much more critical than the displacements.

$$e_e = \left\{ \int_\Omega (\varepsilon^{\mathrm{LPIM}} - \varepsilon^{\mathrm{EXACT}})^{\mathrm{T}} D (\varepsilon^{\mathrm{LPIM}} - \varepsilon^{\mathrm{EXACT}}) \mathrm{d}\Omega \right\}^{1/2} \tag{47}$$

(b) Convergence study

The convergences of MWS are studied. Regularly distributed 18 (3 × 6), 55 (5×11), 112(7×16), 189 (9× 21) and 403(13× 31) nodes are used. The convergence curves with node refinement are shown in Fig. 11. For comparison, the convergence curves for LRPIM and MLPG are also plotted in the same figure. In LRPIM and MLPG methods, all nodes use local weak forms. The h is equivalent to the maximum element size (in x direction) in the FEM analysis in this case. The convergence rates, R, are also given in Fig. 11. The convergence rate is computed via linear regression. From Fig. 11, we can get:

1) Using local weak forms for all nodes, LRPIM and MLPG have better accuracy than the MWS methods. It is because the using strong-forms in the MWS methods will slightly decrease the accuracy.
2) Using MLS, the MWS method has very good convergence rate and the accuracy. Compared with MLPG, MWS with MLS has nearly same convergence and accuracy.
3) The convergence process of MWS using RPIM is not good although the accuracy is acceptable.

The properties of MQ RPIM have been studied by Gu and Liu (2003) in details. It has been found that purely MQ RBF cannot always ensure to exactly reproduce a linear field function. This could be one of the major reasons for the poor h-convergence in using MQ RBF for field variable interpolations. Another reason for a bad convergence is the shape parameters chosen in RBFs. When a proper parameter (C in MQ) is used, the convergence will be improved. Unfortunately, there is no theoretical best value for this parameter. Using MQ RPIM, a strong-form method is more sensitive for the shape parameters than a weak-form method. This is reason that the meshfree weak-form method using RPIM (e.g. LRPIM) usually has good convergence and the MWS method has bad convergence.

To improve the convergence of the MWS based on RPIM, another RBF (e.g. Gaussian RBF, the compactly supported RBFs, etc.) could be used to obtain good h convergence in the future work. However, to find an efficient method to improve the convergence of the RBF interpolations is still an open issue. Some further research is needed about improvement of convergence of the MWS method based on the RPIM.

(c) Efficiency of MWS

In the efficiency study, regularly distributed 55, 189 and 403 nodes are used. The support domain with $\alpha_s = 3.0$ is used to construct shape functions. The CPU time of MWS, LRPIM and MLPG are listed in Table 4. Form this table, it can be found that MWS uses much more less CPU time than LRPIM and MLPG, respectively.

The computational cost must be considered together with the accuracy. A successful numerical method should obtain high accuracy at a lower computational cost. The error–computation time curves of MWS are obtained and plotted in Fig. 12. For comparison, the curve of LRPIM and MLPG is also computed and plotted in the same figure.

It should be noted that the computational cost of a meshfree method mainly comes from three parts:

1) The first part is the cost of interpolation, which mainly comes from computing the inverse of the moment matrix.
2) The second part is the numerical integrations, which mainly determined by the number of Gauss points used.
3) The third part is the cost to solve the finial discrete system equation, which depends on the maximum bandwidth of the global stuffiness matrix.

In our study, the size of the support domain is kept always same. Hence, the cost of the third part is same for MWS, LRPIM and MLPG.

From Fig. 12, the following remarks can be observed:

a) The MLS approximation has better efficiency than RPIM (Liu 2002). Hence, MWS with MLS and MLPG have better efficiency than MWS with RPIM and LRPIM, respectively.
b) For a desired accuracy (such as 10^{-1} error), the cost of MWS methods is lower than corresponding local meshfree methods.

In the MWS method, numerical integrations of a big part of nodes are avoided by the use of the strong form. The more nodes are used to discretize the problem domain, the bigger proportion of nodes use the strong form to avoid numerical integrations. For example, in the case of 403 nodes, less than 150 (one-third) nodes use local weak form. Numerical integrations of two-third of nodes are avoided. The saving of computational

Table 4. CPU time (s)*

	MWS(RPIM)	LRPIM	MWS(MLS)	MLPG
55 nodes	43.7	50.1	2.1	2.1
189 nodes	66.7	310.6	7.3	9.6
403 nodes	123.1	822.7	13.8	24.8

*System: DataMini PC, Intel Pentium 4 CPU 1.80 GHz

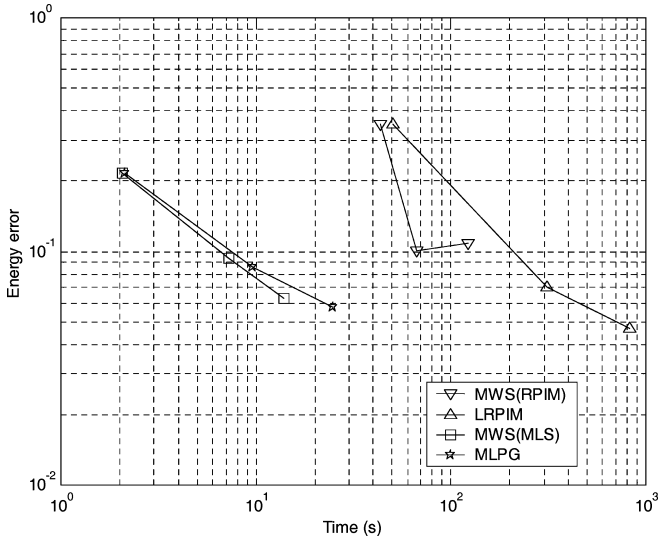

Fig. 12. Computational cost vs. accuracy

cost is considerable. In addition, using the strong form can also save some computational cost for the interpolation because less interpolation points are used.

c) For a given cost (say 20s or 100s), the accuracy of MWS is the better than corresponding local meshfree methods.

Summarizing the above discussions, one can conclude that the efficiencies of MWS methods are better than corresponding local meshfree methods.

Compared with a standard FEM, much more field nodes are usually used in the mesh-free interpolations. The mesh-free interpolation in MWS requires much more computational cost than FEM. In addition, the coefficient matrix in the MWS method is usually asymmetric. In the meantime, the bandwidth of the coefficient matrix in the MWS method is much bigger than that in FEM. Hence, the MWS method is computationally more expensive than FEM. In fact, the computational efficiency is a common issue for most of mesh-free methods. Further research is necessary to improve the efficiency of mesh-free methods.

4.4 Hole in an infinite plate

Consider now a plate with a central circular hole: $x^2 + y^2 \leq a^2$, subjected to a unidirectional tensile load of 1.0 in the x-direction as shown in Fig. 13. Due to symmetry, only the upper right quadrant of the plate is modeled. Plane strain conditions are assumed, and the material constants are $E = 1.0 \times 10^3$, and $\nu = 0.3$. Symmetry conditions are imposed on the left and bottom edges, and the inner boundary of the hole is traction free. The exact solution for an infinite plate with a central

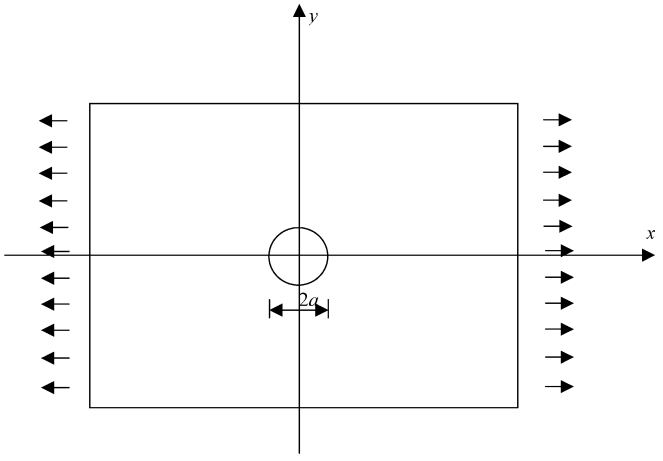

Fig. 13. A plate with a central hole subjected to a unidirectional tensile load

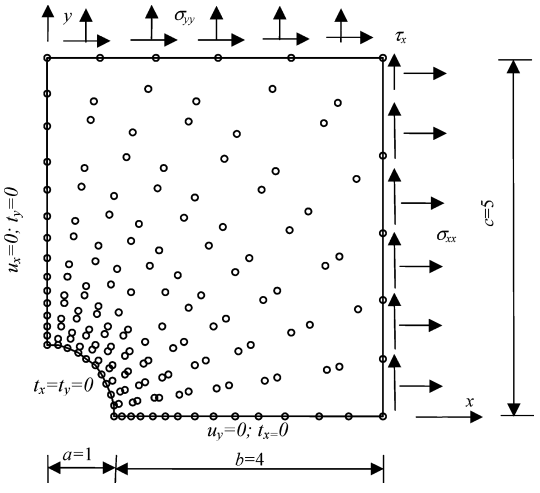

Fig. 14. Nodes and boundary conditions in a plate with a central hole subjected to a unidirectional tensile load in the x direction

circular hole is available. Traction boundary conditions given by the exact solution (Liu and Gu 2001a) are imposed on the right ($x = 5$) and top ($y = 5$) edges. This problem has more complex natural boundary conditions than the beam problem.

The nodal arrangement of 165 nodes is shown in Fig. 14. It is found that the results for the displacements are identical. As the stresses are more critical, detailed results of stresses are presented here. The stress σ_{xx} at $x = 0$ obtained using the MWS is shown in Fig. 15. It can be observed from Fig. 15 that the MWS method yields satisfactory results for this problem considered.

It should mention here that it is very difficult to theoretically prove the stability of the MWS method due

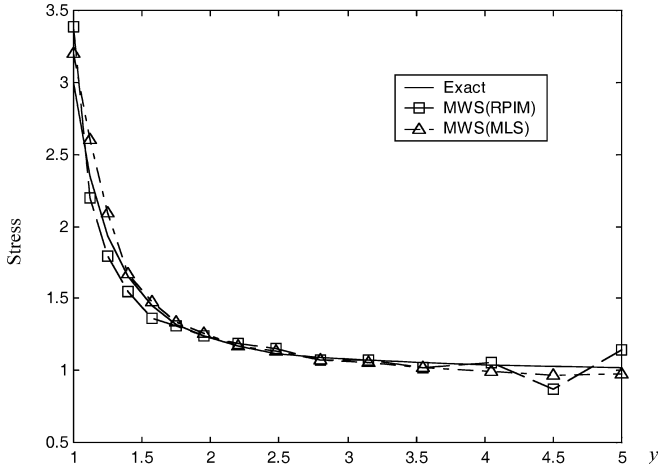

Fig. 15. Stress (σ_{xx}) of the plate obtained by MWS using irregular 165 nodes

to the complexity. Hence, the stability of the MWS method has been demonstrated by some numerical examples. However, these examples are simple benchmark problems. Further studies of the stability of the present MWS method are required, especially to find a theoretical proof.

5 Remarks

A novel meshfree method, the meshfree weak-strong (MWS) form method, is proposed based on a combined formulation of both the strong and local weak forms. The strong form or the collocation method is used for all nodes whose local quadrature domains do not intersect with natural (Neumann) boundaries. Therefore, no numerical integration is required for these nodes. The local Petrov-Galerkin weak-form, which needs the local numerical integration, is only used for nodes on or near the natural boundaries. The natural boundary conditions can then be easily imposed to produce stable and accurate solutions. Numerical examples have demonstrated the effectiveness for elastostatics of the present MWS method. Compared with other meshfree methods, the present MWS method is an improvement for the following reasons:

(a) In MWS, the strong form and local weak form are novelly combined together.
(b) MWS is an efficient meshless method based on the least mesh.
(c) The MWS method fully plays the advantages of meshfree methods based on the strong form and the weak form. It is more accurate and stable than meshfree methods based on the strong form. In the meantime, it is more efficient than meshfree methods based on the weak form.
(d) Numerical examples demonstrate that the present method is very easy to implement, and very flexible and efficient for calculating displacements and stresses of desired accuracy in solids.

As an efficient meshfree method, the present MWS method opens an alternative avenue to develop adaptive analysis codes for stress analysis in solids and structures. Of course, further research work is needed to improve it.

References

Atluri SN, Kim HG, Cho JY (1999) A critical assessment of the truly meshless local Petrov–Galerkin (MLPG), and local boundary integral equation (LBIE) methods. Comput. Mech. 24: 348–372

Atluri SN, Zhu T (1998) A new meshless local Petrov–Galerkin (MLPG) approach in computational mechanics. Comput. Mech. 22: 117–127

Atluri SN, Zhu T (2000) New concepts in meshless methods. Comput. Mech. 22: 117–127

Bathe KJ (2001) The inf-sup condition and its evaluation for mixed finite element methods. Comput. Struct. 79: 243–252

Belytschko T, Lu YY, Gu L (1994) Element-free Galerkin methods. Int. J. Numer. Meth. Eng. 37: 229–256

Cheng AHD, Golberg MA, Kansa EJ, Zammito G (2003) Exponential convergence and H-c multiquadric collocation method for PDE. Numer. Meth. PDE (Submitted)

De S, Bathe KJ (2000) The method of finite spheres. Comput. Mech. 25: 329–345

De S, Bathe KJ (2001) Displacement/pressure mixed interpolation in the method of finite spheres. Int. J. Numer. Meth. Eng. 15: 275–292

Gingold RA, Moraghan JJ (1977) Smooth particle hydrodynamics: theory and applications to non spherical stars. Man. Not. Roy. Astron. Soc. 181: 375–389

Gu YT, Liu GR (2001a) A meshless local Petrov–Galerkin (MLPG) method for free and forced vibration analyses for solids. Comput. Mech. 27: 188–198

Gu YT, Liu GR (2001b) A local point interpolation method for static and dynamic analysis of thin beams. Comput. Meth. Appl. Mech. Eng. 190: 5515–5528

Gu YT and Liu GR (2001c) A meshless local Petrov–Galerkin (MlPG) formulation for static and free vibration analyses of thin plates. Comput. Mech. 246(1): 29–46

Gu YT, Liu GR (2003) A radial basis boundary point interpolation method for stress analysis of solids, Struct. Eng. Mech. Int. J. 15(5): 535–550

Lancaster P, Salkauskas K (1986) Curve and Surface Fitting, an Introduction. Academic Press, London

Liu GR (2002) Mesh Free Methods: Moving Beyond the Finite Element Method. CRC Press, USA

Liu GR, Gu YT (2001a) A point interpolation method for two-dimensional solids. Int. J. Numer. Meth. Eng. 50: 937–951

Liu GR, Gu YT (2001b) A local point interpolation method for stress analysis of two-dimensional solids. Struct. Eng. Mech. 11(2): 221–236

Liu GR, Gu YT (2001c) A local radial point interpolation method (LR-PIM) for free vibration analyses of 2-D solids. J. Sound Vibration 246(1): 29–46

Liu GR, Gu YT (2002) A truly meshless method based on the strong-weak form. In: Proceeding of the 1st Asian Workshop in Meshfree Methods, Liu GR (ed.), Singapore. pp. 259–261

Liu GR, Yan L, Wang JG, Gu YT (2002) Point interpolation method based on local residual formulation using radial basis functions. Struct. Eng. Mech. 14(6): 713–732

Nayroles B, Touzot G, Villon P (1992) Generalizing the finite element method: diffuse approximation and diffuse elements. Comput. Mech. 10: 307–318

Powell MJD (1992) The theory of radial basis function approximation in 1990. In: Advanced in Numerical Analysis, Light FW (ed.), pp. 303–322

Schaback R, Wendland H (2000) Characterzation and construction of radial basis functions. In: Multivariate Approximation and Applications, Dyn N, Leviatan D, Levin D, Pinkus A, (eds.) Cambridge University Press

Wendland H (1998) Error estimates for interpolation by compactly supported radial basis functions of minimal degree. J. Approx. Theory 93: 258–396

Zhang X, Liu XH, Song KZ, Lu MW (2001) Least-square collocation meshless method. Int. J. Numer. Meth. Eng. 51(9): 1089–1100

Zhu T, Zhang JD, Atluri SN (1998) Local boundary integral equation (LBIE) method in Computational mechanics, and a meshless discretization approach. Comput. Mech. 21(3): 223–235

Zong Z (2003) A complex variable boundary collocation method for plane elastic problems. Comput. Mech. 31: 284–292

Wu YL, Liu GR, Gu YT (2002) Application of meshless local Petrov–Galerkin (MLPG) approach to simulation of incompressible flow. Comput. Fluids (Submitted)